

Towards an autonomous self-tuning vibration energy harvesting device for wireless sensor network applications

This article has been downloaded from IOPscience. Please scroll down to see the full text article.

2011 Smart Mater. Struct. 20 025004

(<http://iopscience.iop.org/0964-1726/20/2/025004>)

View [the table of contents for this issue](#), or go to the [journal homepage](#) for more

Download details:

IP Address: 67.81.148.151

The article was downloaded on 08/01/2011 at 07:59

Please note that [terms and conditions apply](#).

Towards an autonomous self-tuning vibration energy harvesting device for wireless sensor network applications

Vinod R Challa, M G Prasad and Frank T Fisher

Department of Mechanical Engineering, Stevens Institute of Technology, Hoboken, NJ 07030, USA

E-mail: vchalla@stevens.edu and ffisher@stevens.edu

Received 8 June 2010, in final form 3 December 2010

Published 6 January 2011

Online at stacks.iop.org/SMS/20/025004

Abstract

Future deployment of wireless sensor networks will ultimately require a self-sustainable local power source for each sensor, and vibration energy harvesting is a promising approach for such applications. A requirement for efficient vibration energy harvesting is to match the device and source frequencies. While techniques to tune the resonance frequency of an energy harvesting device have recently been described, in many applications optimization of such systems will require the energy harvesting device to be able to autonomously tune its resonance frequency. In this work a vibration energy harvesting device with autonomous resonance frequency tunability utilizing a magnetic stiffness technique is presented. Here a piezoelectric cantilever beam array is employed with magnets attached to the free ends of cantilever beams to enable magnetic force resonance frequency tuning. The device is successfully tuned from -27% to $+22\%$ of its untuned resonance frequency while outputting a peak power of approximately 1 mW. Since the magnetic force tuning technique is semi-active, energy is only consumed during the tuning process. The developed prototype consumed maximum energies of 3.3 and 3.9 J to tune to the farthest source frequencies with respect to the untuned resonance frequency of the device. The time necessary for this prototype device to harvest the energy expended during its most energy-intensive (largest resonant frequency adjustment) tuning operation is 88 min in a low amplitude 0.1g vibration environment, which could be further optimized using higher efficiency piezoelectric materials and system components.

(Some figures in this article are in colour only in the electronic version)

1. Introduction

Wireless sensor networks have attracted an increasing interest due to their ease of implementation in inaccessible locations and have the flexibility to be embedded with any system of interest without the cost and inconvenience of wiring. While traditional wireless sensors are powered by conventional batteries, vibration energy harvesting promises to have the ability to power these sensors in a cost effective manner over time. Typically, vibration energy is converted to electrical energy by using electrostatic, electromagnetic, or piezoelectric transduction mechanisms. Examples of electrostatic-based energy harvesting devices include the devices built by Roundy [1], Mitcheson [2], and Chiu [3]. Similarly,

electromagnetic based energy harvesting devices have been developed by Williams [4], Glynne-Jones [5], and Beeby [6]. While milliscale piezoelectric based devices were developed by Roundy [7], Ericka [8], and Kim [9, 10], recently much work has been done in developing MEMS based piezoelectric devices [11–15]. Researchers such as Wang *et al* [16] and Berbyuk *et al* [17] have developed magnetostrictive based models and devices for active vibration energy harvesting. Recently, the current authors have presented a coupled energy harvesting technique (i.e. which can include multiple transduction mechanisms within a single energy harvesting device) to improve the power output through matching the electrical damping with the mechanical damping [18]. A bistable inertial oscillator comprised of permanent magnets

and a piezoelectric cantilever beam is presented that utilizes the nonlinear behavior of the system [19]. A similar setup has been made using a piezoelectric cantilever for enhanced power output through coupling to a static magnetic field [19, 20].

While vibration energy harvesting is promising, there exist several challenges that need to be addressed for efficient energy harvesting. One such major challenge is to have the energy harvesting device in resonance with the source frequency. Gieras *et al* have described a technique where the length of the cantilever can be altered to adjust the resonance frequency [21], while Wu *et al* have used a similar technique to move the tip mass for tuning purposes [22]. Other methods include actively tuning the resonance frequency by applying an electrical potential to alter the beam stiffness through electrostatic, piezoelectric and thermal methods [23, 24], while the application of an axial load to change the stiffness and thus alter the resonance frequency has also been discussed [25]. Recently, the authors have proposed a magnetic force resonance frequency tuning technique which allows one to tune the natural frequency of the energy harvesting beam to match both lower and higher source frequencies [26]. The nonlinearity of piezoelectric materials has also been used to passively tune MEMS energy harvesting devices [27]. A summary of these approaches is discussed in a recent review of the principles and operating strategies for increasing the operating frequency range of vibration-based micro-generators [28]. Adapting these techniques to a self-tunable energy harvesting device would enable the device to tune its natural frequency by itself without user intervention.

In this paper, a self-tunable energy harvesting device is presented that utilizes the piezoelectric technique for energy harvesting and the magnetic force tuning technique [26] for resonance frequency tunability. The tuning technique involves adjustment of magnetic stiffness through the application of magnetic forces to alter the overall effective stiffness of the vibrating cantilever beam. The change in stiffness can be used to adjust the resonance frequency of the device to match the source frequency for peak power output. The induced stiffness is either positive or negative depending on the mode of the magnetic force (repulsive or attractive) employed. An attractive force lowers the resonance frequency of the beam, while a repulsive force increases the beam's resonance frequency. The tuning process is performed by means of an actuator that is programmed to periodically adjust the distance between magnets to introduce the necessary amount of magnetically induced stiffness in the system to tune the device resonance frequency to a desired source frequency (i.e. that of the forcing frequency). The energy consumed by the actuator and the time to recover the expended energy in performing the tuning are also discussed.

2. Theoretical work

In the following sections, the magnetic force resonance frequency tuning technique is briefly presented, which allows the device to alter its resonance frequency to match various source frequencies within an allowable frequency bandwidth. Later a theoretical model relating the effect of distance

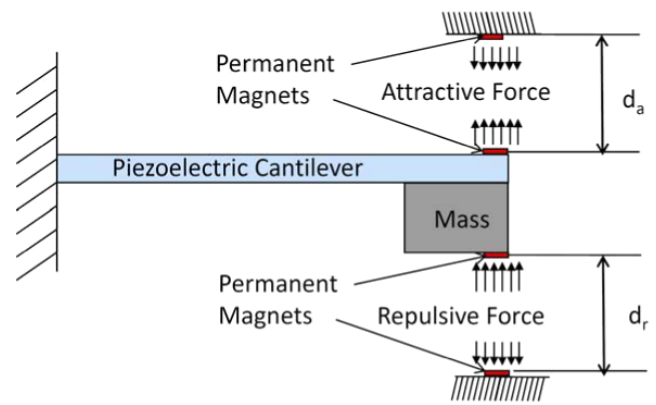


Figure 1. Schematic of the variable magnetic stiffness resonant frequency tuning technique [26].

between the magnets to the amount of magnetic stiffness induced in the system and the corresponding change in device resonance frequency is presented. At the end of section 2, the piezoelectric cantilever array device is presented along with the power equations and energy consumption of the actuator.

2.1. Magnetic force resonance frequency tuning technique

Here a magnetic force is employed to induce the desired amount of magnetic stiffness into the system, thereby altering the device resonance frequency. This technique was previously presented along with experimental validation by the authors [26]. While the resonance frequency tuning technique can be employed on any structure, here a cantilever beam with tip mass is considered as the vibrating structure. Magnets are placed at the top and bottom of the cantilever beam at the tip, such that they are aligned with the magnets on the device enclosure and arranged such that either a magnetic force of attraction or repulsion can be applied (see figure 1). The distance between the magnets dictates the amount of magnetic force exerted on the cantilever beam, which thereby would induce an additional magnetic stiffness in the system and hence alter the resonance frequency of the device. The mode of magnetic force determines the type (positive or negative) of magnetic stiffness induced on the cantilever beam; a magnetic force of attraction would induce a negative stiffness and thus lower the device's natural frequency, whereas a magnetic force of repulsion induces a positive stiffness that increases the total stiffness in the device and hence increases the device's resonant frequency. The technique allows one to tune the resonance frequency of the beam to match both lower source frequencies and higher source frequencies by simply applying the desired mode of magnetic force.

2.2. Magnetic stiffness and its effect on resonance frequency

While magnets of different geometries can be employed to induce the desired force, cylindrical magnets are used here. The resulting magnetic force between two cylindrical magnets

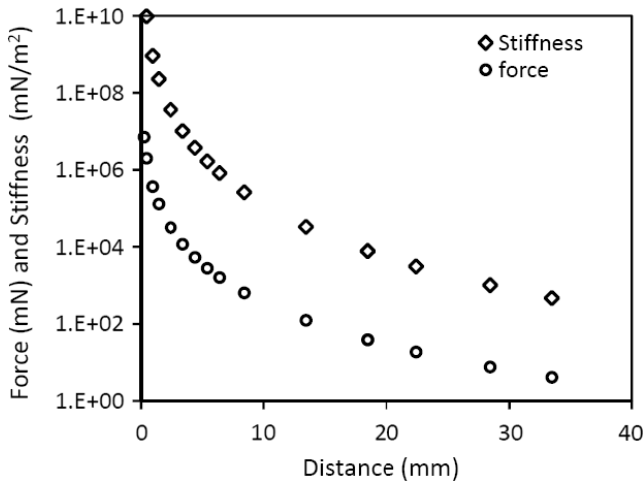


Figure 2. Theoretical magnitude of the magnetic force and stiffness versus separation distance between two cylindrical magnets (the values used are listed in table 1).

is given as

$$F_{\text{mag}}(d) = \left[\frac{B_r^2 A_m^2 (l+r)^2}{\pi \mu_0 l^2} \right] \left[\frac{1}{d^2} + \frac{1}{(d+2l)^2} - \frac{2}{(d+l)^2} \right] \quad (1)$$

where B_r is the residual flux density of the magnet, A_m is the common area between the magnets, l is the length of the magnet, r is the radius of the magnet, d is the distance between the magnets, and μ_0 is the permeability of the intervening medium. The associated magnetic stiffness is equal to the change in magnetic force with the change in distance between the magnets. The value of the stiffness is positive for repulsive magnetic force and negative for attractive magnetic force based on the direction of the force and is given as

$$K_{\text{mag}}(d) = \frac{\pm \delta F}{\delta d} = \frac{\pm \partial F}{\partial d}. \quad (2)$$

By substituting equation (1) in (2), the magnitude of the magnetic stiffness is given as

$$K_{\text{mag}}(d) = \left| \frac{B_r^2 A_m^2 (l+r)^2}{\pi \mu_0 l^2} \left[-\frac{2}{d^3} - \frac{2}{(d+2l)^3} + \frac{4}{(d+l)^3} \right] \right|. \quad (3)$$

From equation (3) the magnetic stiffness can be varied by altering the magnetic flux density, the common area between the magnets, and the distance between the magnets. In application the common area between the magnets would be a difficult choice, as the area of the magnets used is very small which requires high precision to obtain the desired magnetic force. Hence the distance between the magnets is chosen to alter the force and corresponding stiffness. An example of a plot of magnetic force and the corresponding stiffness versus distance between magnets is shown in figure 2 suggesting that the magnitude of the force and the stiffness are nonlinear with respect to the distance between the magnets. Although the distance between the magnets varies slightly as the structure vibrates, this effect is relatively small and the slope of the magnetic stiffness is relatively flat over the distances used

Table 1. Descriptions of the variables and their values.

Symbol	Description	Value	Units
B_r	Residual flux density	1.1	Tesla
A	Area of magnet	25.128	mm ²
l	Length of the magnet	2	mm
r	Radius of the magnet	4	mm
μ_0	Permeability of air	1.256×10^{-6}	H m ⁻¹
A_m	Common area between magnets	25.128	mm ²
E	Young's modulus	3.81×10^{10}	Pa
I	Moment of inertia	3.6×10^{-13}	kg m ²
L	Length of the beam	480	mm
b	Width of the beam	20	mm
h	Thickness of the beam	0.6	mm
m_{eff}	Effective mass of the beam	25.6	g
d_{31}	Strain coefficient of piezoelectric material	1.75×10^{-10}	C N ⁻¹
ϵ	Dielectric constant	1.55×10^{-8}	F m ⁻¹
Cp	Capacitance	1.7×10^{-7}	F
t_p	Thickness of piezoelectric layer	0.16	mm

to tune the resonant frequency (here the tuning ranges are greater than 10 mm as shown in figure 4). Hence as a first-order approximation, the change in separation distance due to vibration of the cantilever is neglected here. The associated values of the variables used are listed in table 1.

2.3. Effect of magnetic force on resonance

In the case of no magnetic force, the effective stiffness associated with the cantilevered beam is given as

$$K_{\text{beam}} = \frac{3EI}{L^3} = \frac{Ebh^3}{4L^3} \quad (4)$$

where E , L , b , h are the effective Young's modulus, length, width and thickness of the beam. Here the effective Young's modulus of the multilayered beam used is that provided by the manufacturer. The corresponding natural frequency of the cantilevered beam is given as

$$\omega = \sqrt{\frac{K_{\text{beam}}}{m_{\text{eff}}}} \quad (5)$$

where m_{eff} is the effective mass of the beam and is equal to the tip mass (m_{tip}) plus 0.23 times the mass of the beam (m_{beam}). For the case of an applied magnetic force, there is an additional stiffness that is introduced to the energy harvesting device. The resonance frequency of the device is now a function of beam stiffness and the stiffness associated with the magnetic force and is given as

$$K_{\text{eff}} = K_{\text{beam}} + K_{\text{mag}} \quad (6)$$

(note that $K_{\text{mag}} < 0$ for repulsive magnetic force and $K_{\text{mag}} > 0$ for attractive magnetic force). Based on the mode of magnetic force (repulsive or attractive) induced, the total effective stiffness of the device would increase or decrease. The natural frequency of the device is now a function of the effective stiffness given in equation (4), and thus the resonant frequency of the device is given as

$$\omega = \sqrt{\frac{K_{\text{eff}}}{m_{\text{eff}}}} \quad (7)$$

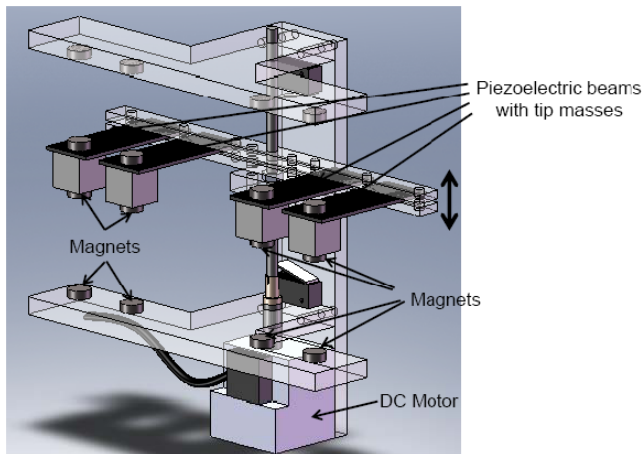


Figure 3. Schematic of the self-tunable piezoelectric beam array energy harvesting device with a programmable motor controller.

The amount of magnetic force that can be induced is limited by the yield strength of the beam (see [26] for a detailed explanation). The tunable range is thus not only dependent on the amount of magnetic force that can be induced but also on the desired lowest peak power output (i.e. the cut-off power output). It is to be noted that the amount of deflection of the beam due to magnetic stiffness is considered negligible, and deformation of the cantilever beam due to the application of the magnetic force is not considered when calculating the desired separation distance of the magnets.

2.4. Self-tunable energy harvesting device

Moving towards an autonomous, self-tunable magnetic force resonance tuning technique, a proof of concept prototype has been developed as shown in figure 3. The device is made of four piezoelectric cantilever beams with equal tip masses and magnets attached at the top and bottom, such that all the beams exhibit (approximately) the same natural frequency. The beam array is mounted on a fixture that is fixed onto a threaded rod (whose threads per inch and diameter dictate the velocity of travel) that is further fixed on a DC motor/actuator as shown in figure 3. As the motor rotates, the fixture is displaced either up or down based on the flow of current in the motor. The other magnets required to induce magnetic force/stiffness are attached to the fixed ends of the device as shown in figure 3.

When the beam array is subjected to a known base vibration excitation, the beams vibrate at the source frequency whose value is known from the voltage output of the beams. The frequency at which the voltage is produced corresponds to the frequency of vibration. If this source frequency is the same as the natural frequency of the beam (which is known in theory based on the beam geometry and properties), then the beam is in resonance. Hence no magnetic stiffness is required and for maximum energy harvested the beam would remain at the same location (position). When the source frequency is different from the natural frequency of the beam, the difference in frequencies is evaluated and a command is given to the motor to move the beam to the distance necessary

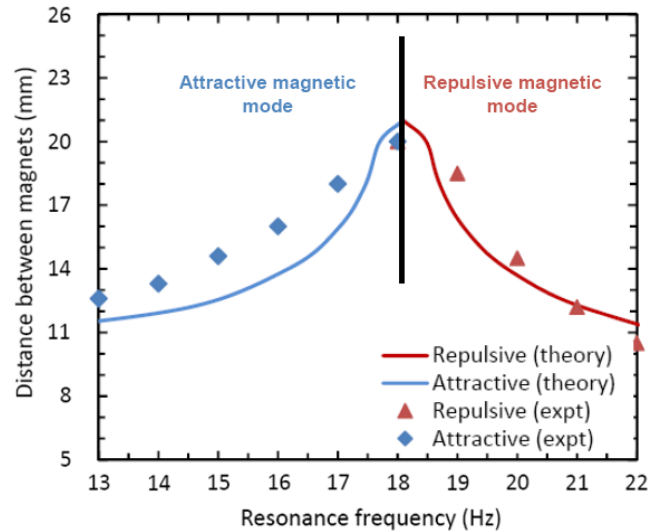


Figure 4. Relationship between the effective resonance frequency of the device and the separation distance of the magnets (the system parameters are as given in table 1).

to induce the desired amount of additional magnetic stiffness into the system. The distance between the appropriate magnets and the resulting tuned resonance frequency of the device are estimated from equations (3), (6), and (7) and compared with experimentally determined values as shown in figure 4 (further discussion of the experimental results from this work is given in section 3). It is to be noted that the theoretical maximum deflection of the beam due to magnetic stiffness at the extreme tuned frequency is 2.7 mm. The equilibrium point is determined by measuring the static deflection of the beam with a scale bar. The distance d is now the distance between the two centers of mass of the magnets placed on the beam and the fixed end. The difference in experimental and theoretical values in figure 4 can be explained by the experimental errors in measuring the equilibrium point.

2.5. Power output from the piezoelectric cantilever beam

The piezoelectric cantilever beam produces a voltage V due to the mechanical stress σ from the induced vibrations in the beam, which can be written as

$$V = \frac{-d_{31}t_p\sigma}{\varepsilon} \quad (8)$$

where t_p is the thickness of the piezoelectric layer, σ is the average stress in the piezoelectric layer, $-d_{31}$ is the piezoelectric strain constant, and ε is the dielectric constant of the piezoelectric material. While a composite cantilever beam is employed, the equations provided here are generic and can be employed for any geometry. For piezoelectric composite cantilever specific equations, the reader is referred to the earlier work done by the authors [18]. The corresponding power output is given as

$$P = \frac{V^2 R_L}{(R_S + R_L)^2} \quad (9)$$

where R_S is the impedance of the piezoelectric cantilever beam (also referred to as the source resistance)

$$R_S = \frac{1}{\omega C_p} \quad (10)$$

and R_L is the load resistance. Note that when $R_S = R_L$, a condition termed impedance matching [29], the device power output is optimal, which is given as

$$P = \frac{V^2}{4R_S}. \quad (11)$$

2.6. Energy consumed by the actuator

In displacing the cantilever beam array to the desired distance (magnetic separation) for resonance frequency tuning, an amount of energy is consumed by the actuator. The amount of energy consumed would largely depend on the distance traveled by the beam array. Theoretically, the energy required to displace the beam can be determined as follows:

$$E_{\text{actuator}} = \pm \int_{x_i}^{x_f} m_{\text{array}} g \, dx \pm \int_{x_i}^{x_f} F_{\text{mag}} \, dx \quad (12)$$

where m_{array} is the mass of the array (including all portions of the system which are moved during the tuning operation) and x_i and x_f are the initial and final positions of the beam array for a given tuning step. The energy consumed is very much dependent on the direction of motion, position of the beam array and the mode of the magnetic force. It would be optimal to have a magnetic force of attraction at the top of the device as it would reduce the effort of working against gravity and, similarly, implementing the repulsive mode at the bottom of the cantilever beam would reduce the effort of working against the magnetic force by utilizing gravity in its favor. For a case where the velocity of travel of the actuator is constant and is not influenced by the changes in magnetic force, the time required to displace the cantilever beam array to the desired location can be given as

$$t = \frac{x_f - x_i}{v_m} \quad (13)$$

where x_f and x_i are the final and initial positions of the beam array and v_m is the velocity of the actuator. Upon evaluating the time required, the total electrical energy E_{in} consumed by the actuator can be given as

$$E_{\text{motor}} = t V_{\text{in}} I_{\text{in}} \quad (14)$$

where V_{in} is the input voltage to the motor and I_{in} is the electrical current in the motor. This energy is the total energy supplied by the source and is largely governed by the efficiency of the motor (the efficiency of the motor used in this initial prototype is approximately 35% as per company specifications) and the effectiveness of the employed technique. Based on the desired tunable range and the precision of tuning, an appropriate motor can be chosen to efficiently perform the self-tunable technique.

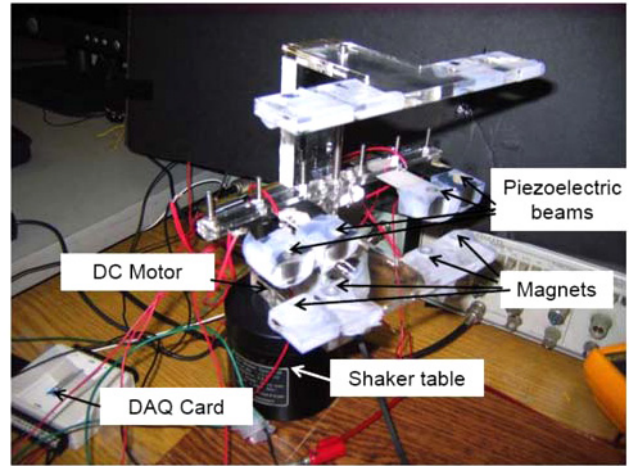


Figure 5. Self-tunable energy harvesting device.

3. Experiment

To demonstrate the autonomous self-tunable technique described above, four piezoelectric cantilever beams (APC International Ltd stripe actuators) are employed for the energy harvesting device. Tip masses of equal mass are inserted on all the four beams to lower the beam natural frequencies and also to maximize the power output of each beam. The beams are assumed to exhibit the same natural frequency as described in section 2. Common cylindrical magnets (Radio Shack) are used to exert the required magnetic stiffness to tune the beams to different resonance frequencies and are placed on the device as shown in figure 5. The beam array is mounted on an assembly where the actuator can displace the beam array vertically to the desired location. The actuator employed is a simple DC motor (Lego motor 43362) whose direction of motion is dictated by the flow of current through the motor. The distance by which the beam array is displaced depends on the time and velocity of the actuator. It is to be noted that during the repulsive magnetic mode the magnetic force acts in the direction opposite to the motion of the actuator, whereas in the case of the attractive mode, the magnetic force acts in the same direction as the actuator, thus requiring less energy as compared to the repulsive mode. Hence having the attractive magnetic mode at the top and the repulsive mode at the bottom would be advantageous as the force of gravity would assist the motor. The built device is mounted on an electrodynamic mini shaker (Bruel and Kjaer) and the lead wires from the piezoelectric beams are connected to the data acquisition (DAQ) card (National Instruments) that in turn is connected to the computer by a USB cable.

The motor/actuator is powered from the DAQ card and is controlled by the H-bridge (see figure 6) to dictate the direction of flow of current in the motor. The H-bridge is formed using relay switches that are turned on/off by the DAQ card that is in turn is controlled by the LabView software. The voltages and frequencies of the beam array are monitored in real time to ensure that the device is in resonance and is producing peak power output. The input frequency and acceleration

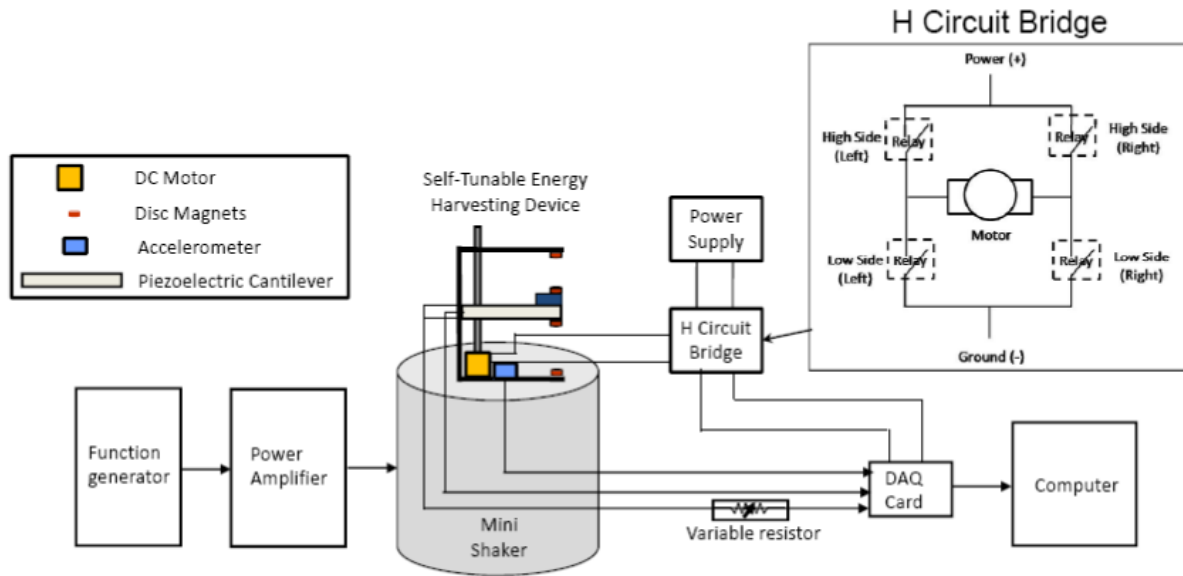


Figure 6. Layout of the experimental setup.

are provided by a function generator (HP 4120 series) and power amplifier (Bruel and Kjaer) connected to the shaker. The theoretical relationship between the distance between the magnets and the resulting frequency shift of the piezoelectric beams is known from figure 4, and is provided to the program for the desired frequency tuning operation. As the source frequency is altered, the beam array is moved accordingly to induce the required magnetic stiffness required to tune the device to the source frequency (see equation (6)). The purpose of the accelerometer is to determine the source acceleration initially (a one-time measurement); hence the power consumed is negligible and is not accounted for in the analysis. The complete layout of the experiment detailing the electrical and mechanical components of the system is illustrated in figure 6.

As discussed in section 2.5, to obtain the peak power output of the piezoelectric energy harvesting device, the load resistance has to match the beam impedance. Experimentally the beam impedance (optimal load resistance) value is determined by performing a load resistance sweep test for each individual beam while monitoring the power output of the corresponding piezoelectric beam; at peak power output the employed load resistance value is the impedance in the beam. The damping generated during the no-load condition is considered to be purely mechanical, as there is no energy harvested. By having a resistive load, energy is generated due to the piezoelectric property and hence the corresponding damping is referred to here as piezoelectric damping. In another sense, the energy generated due to the piezoelectric technique is referred to as the piezoelectric damping which is accounted towards the electrical damping. Hence the difference in damping values between the no-load and load conditions would provide us with the damping due to the energy harvesting (electrical damping). The average of the damping and optimal resistance values is used as the corresponding value of the beam array device. Here the optimal load resistances are manually adjusted to account for

changes in resonance frequencies as the device is in operation; for a fully autonomous device such changes would need to be programmed accordingly as part of the tuning step; this will be implemented in future work.

4. Results and discussion

4.1. Optimal resistance versus tuned resonance frequency

The voltage and power output produced from the piezoelectric beam array is captured across a varying load resistance to determine the peak power output and the optimal load resistance. An example of a plot of power output versus load resistance at the untuned resonance frequency of a single piezoelectric beam in the array is presented in figure 7(a). Here a peak power output of $250 \mu\text{W}$ is produced at an optimal load resistance value of $47 \text{ k}\Omega$ at an untuned resonance frequency of 18 Hz. Similar experiments are performed for each individual beam in the array at different magnetically tuned resonance frequencies (by adjusting the separation distance between the magnets) to determine the optimal resistance values at each resonance frequency. These average values are plotted in figure 7(b) and are compared to the theoretical impedance value of the beam at various resonance frequencies that are calculated using equation (10).

4.2. Damping versus tuned resonance frequency

As presented by the authors in their earlier work on the magnetic force/stiffness resonance frequency tuning technique [26], with resonance frequency tuning an additional magnetic damping is introduced into the system which alters the total damping in the system. Thus the total damping value at each tuned resonant frequency is obtained by performing a flick test (the beam is flicked at its tip and its amplitude is allowed to decay with time) under an optimal resistive loading

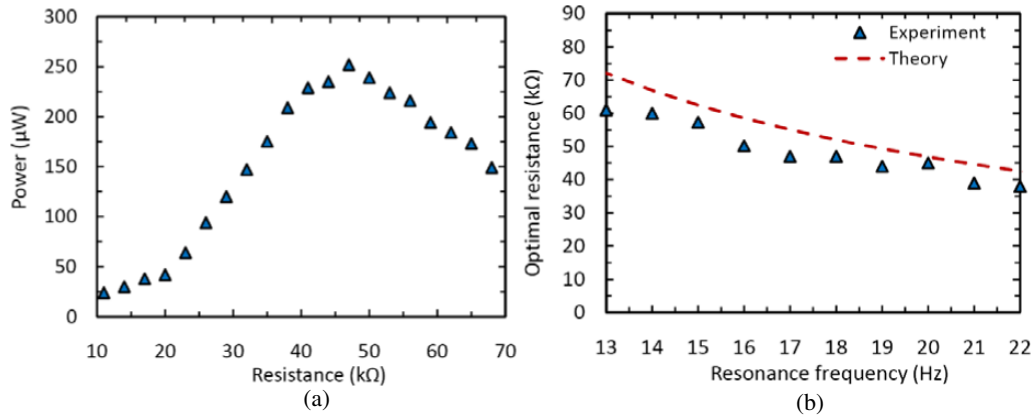


Figure 7. (a) Power output versus load resistance at 18 Hz, and (b) load resistance versus resonance frequency.

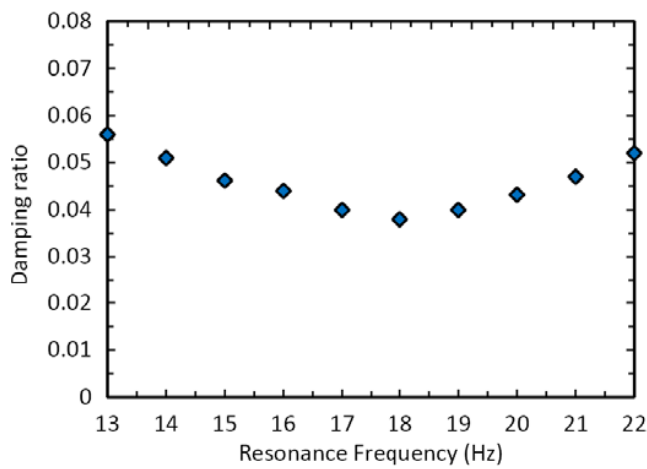


Figure 8. Average total damping values (mechanical plus electrical) of the beam array versus resonance frequency.

condition to obtain an amplitude decay plot, and is calculated as

$$\zeta = \frac{1}{2\pi n} \ln \left(\frac{a_1}{a_2} \right) \quad (15)$$

where n is the number of periods between the amplitudes a_1 and a_2 . It is observed that irrespective of the mode of magnetic force induced, the damping in the system increases with increasing magnetic stiffness. The initial average damping value obtained from all the beams in the system is found to be 0.038 with no magnetic force/stiffness induced. As the device was tuned to the farthest frequencies in the tunable range, the damping value increased to 0.056 on the attractive side and to a value of 0.052 on the repulsive side, as shown in figure 8.

4.3. Device power output versus tuned resonance frequency

The power generated from the cantilevered beam array has been measured with respect to the various source frequencies for which the device is tuned to be in resonance. The untuned natural frequency of the beam array is 18 Hz (all beams are designed to be at this natural frequency) outputting a peak power of approximately 1 mW at 0.1g acceleration. The

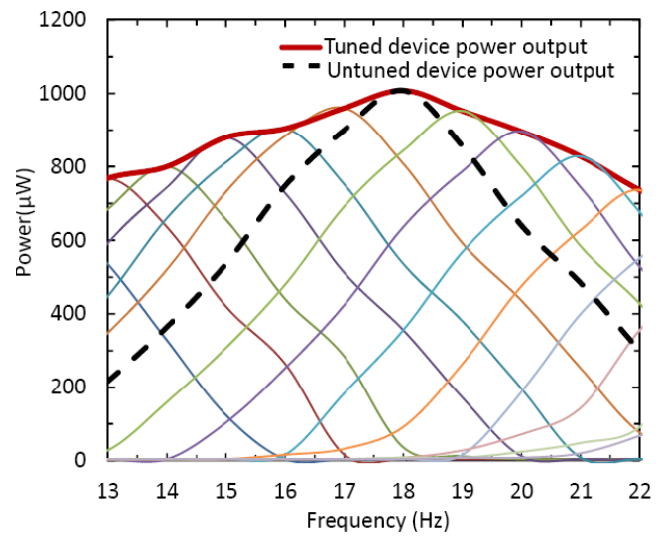


Figure 9. Experimental power output versus resonance frequency of the four-beam array device. The thick dashed line shows the power–frequency curve for a four-beam array with no magnetic tuning. Power–frequency curves for the system tuned to various resonant frequencies are also shown. The thick red line indicates the optimal power output of the device if it were to be tuned to resonance at the respective source frequency.

power output from the beam array drops tremendously as the source frequency is shifted away from 18 Hz, emphasizing the importance of resonance on the power output of the device. As the source frequency is altered between 13 and 22 Hz, the beam array is tuned to resonate accordingly by inducing the desired magnetic stiffness, and the corresponding power output is noted at each of the tuned frequencies. The total power output harvested varies from 768 μW to 1 mW on the attractive side and from 736 μW to 1 mW on the repulsive side as shown in figure 9.

The results shown in figure 9 arbitrarily assume the root mean square (rms) of peak power output as the cut-off power to determine the frequency tunable range of the device. The device can be tuned to lower or higher resonant frequencies than those shown in figure 9, albeit with a further decrease in output power. Taking into account the value of the

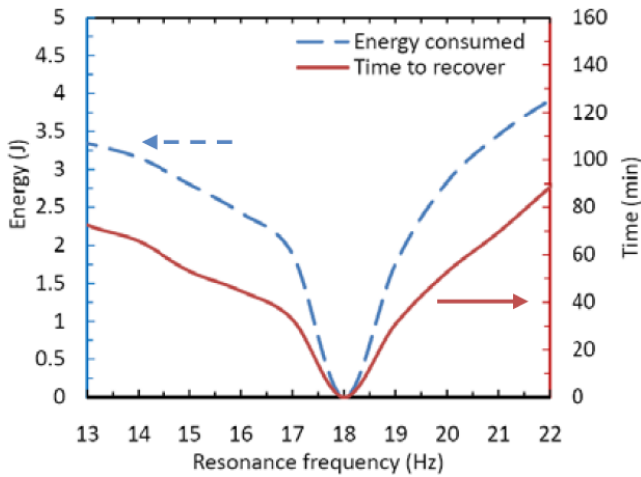


Figure 10. Energy consumed by the actuator and the time taken for the device to recover the energy.

cut-off power for resonance frequency tunability of 0.707 assumed here, a frequency bandwidth of 9 Hz is obtained, corresponding to 49% frequency tunable range. The red line in figure 9 indicates the maximum power output of the device when tuned to particular frequencies and can be compared with the dotted line representing the untuned harvesting device.

4.4. Energy consumed by the actuator and time to reclaim the energy

The energy consumed by the actuator to tune the piezoelectric beam array is evaluated experimentally as shown in figure 10. The amount of energy consumed depends on the distance through which the beam array has to be displaced to induce the desired magnetic stiffness and the efficiency of the actuation technique and components. It is to be noted that the voltage supplied to the motor is limited by the output voltage of the DAQ card, which is a drawback for an efficient tuning mechanism. The velocity of travel of the beam array fixture when subjected to a 5 V and 0.12 A input to the motor is determined to be 2.67 mm s^{-1} through several experiments. This velocity is used to determine the time required to move the beam array to the desired locations expected to theoretically ensure that the device remains in resonance with the source frequency (see figure 4). From the time obtained to tune to a particular frequency, the total energy consumed is evaluated. The amount of electrical energy consumed was found to be 3.2 J–3.9 J when tuned from the initial untuned resonance frequency position of the beam array to 13 Hz and 22 Hz, respectively. The corresponding time required by the device to recover this energy is theoretically evaluated based on the power output at that specific tuned frequency as shown in figure 10. Approximately 72 min is required to recover the energy spent when the device is tuned to 13 Hz and 88 min when tuned to 22 Hz. The energy consumed in the repulsive mode is slightly greater than the energy consumed in the attractive mode due to the work done against the magnetic force to induce the desired magnetic stiffness as explained in section 3.

4.5. Effectiveness of a tuning approach for increasing the net power harvested by the system

Here it is desirable to evaluate the effectiveness of the tuning approach for increasing the net electrical power harvested by the system (referring specifically to the net electrical energy harvested that is available to be used by other components of the overall system, such as sensor powering, wireless communication, etc). To do so one must take into account both the additional electrical energy generated due to the system being at resonance over a larger range of frequencies, as well as accounting for the amount of electrical energy that is spent due to the actuation of the tuning mechanism. For the sake of comparison, here one can contrast the net electrical energy harvested from the system described in this work with a simple four-beam array with discrete frequencies selected to span the same frequency bandwidth as obtained for the current device; we will refer to the comparison system as a discrete beam array (see figure 11). For the discrete beam array, the individual cantilevers are designed to have different resonance frequencies; for example, by varying the lengths of the individual beams (recall that in the current tunable design described here, the cantilever beams each have the same initial resonance frequency). For simplicity we assume that each of the individual cantilever beams is designed such that the resonant frequencies span the frequency bandwidth. While the discrete beam array approach is effective in increasing the frequency bandwidth over which the device is able to harvest appreciable levels of energy, by its very design this approach guarantees that only one of the elements in the beam array will be in resonance at a given frequency. For the tunable resonance frequency approach described herein to be more efficient than the discrete beam array, such a device must be able to harvest more net energy than the discrete beam array device over time, accounting for the energy that must be consumed for tuning purposes.

Thus for the sake of comparison a discrete multibeam array consisting of cantilever beams having resonance frequencies of 14.5, 16.5, 18.5 and 20.5 Hz (chosen such that both approaches have a similar bandwidth) is considered as shown in figure 11. Here the theoretical power output for the discrete multibeam array is simply the sum of the power harvested by each individual beam at a given source frequency under optimal loading conditions (i.e. impedance matching) using equations (9)–(11) and the parameters given in table 1. A value of 0.1g is used for the acceleration amplitude to match the experimental source vibration conditions.

The theoretical power output of the discrete multibeam array is shown in figure 11, where it is compared to the performance of the tunable device based on the magnetic stiffness tuning approach (experimental results shown earlier in figure 9). The discrete multibeam array demonstrated a maximum power of $803 \mu\text{W}$ at approximately 16 Hz, where of this total power approximately $165 \mu\text{W}$ is provided by the 14.5 Hz beam, $259 \mu\text{W}$ by the 16.5 beam, $218 \mu\text{W}$ by the 18.5 Hz beam, and finally $160 \mu\text{W}$ by the 20.5 Hz beam. Note that the results for the discrete array are not symmetric about the midpoint of the frequency span. By comparison, the maximum power of the tunable array is

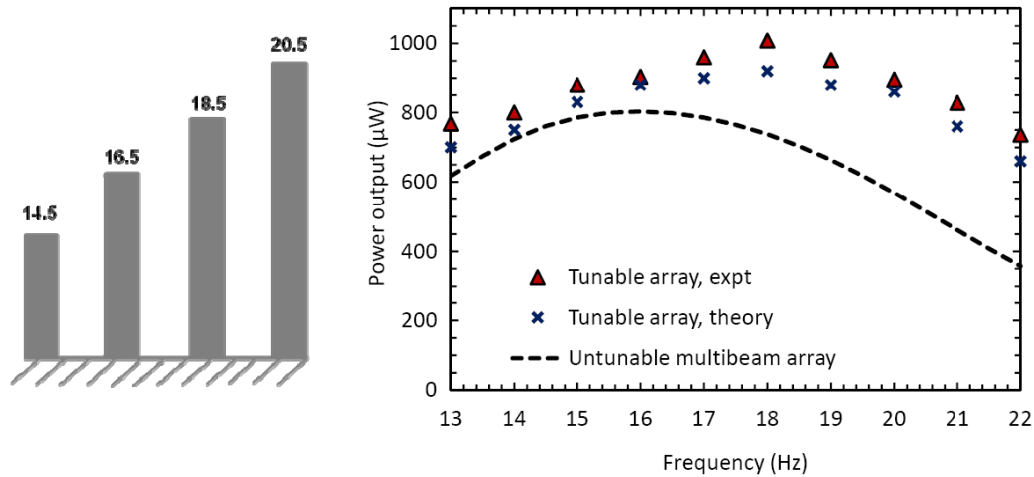


Figure 11. (Left) A four element discrete multibeam array with different resonant frequencies selected to span the desired bandwidth. (Right) Comparison of the power output of the tunable energy harvesting four-beam array (experimental and theoretical) versus the theoretical power output of the discrete four element multibeam array shown on the left.

approximately 1 mW at around 18 Hz (here all four beams in the array are in resonance), with a significant increase in power output versus the discrete multibeam array over the complete frequency bandwidth from 13 to 22 Hz. At a source frequency of approximately 16 Hz, where the discrete beam array has a theoretical maximum power output of $803 \mu\text{W}$, the experimentally determined power out of the four-beam tunable array is $904 \mu\text{W}$ (note that this power output is less than the maximum total power output of approximately 1 mW at 18 Hz due to additional damping introduced into the system when the magnetic stiffness is applied as shown in figure 8).

Note that figure 11 does not include the energy consumed in tuning the device. The total net energy harvested, E_{net} , can be calculated by subtracting the amount of energy spent to tune the device (see equation (14)) from the amount of electrical energy harvested such that

$$E_{\text{net}} = E_{\text{harvested}} - E_{\text{tuning}}. \quad (16)$$

The net energy harvested by the discrete multibeam array is calculated by integrating the average power harvested over the entire frequency bandwidth ($638 \mu\text{W}$) over time and is plotted in figure 12. Also shown in figure 12 are the effective net energies harvested by the tunable device array at different resonant frequencies assuming that a one-time tuning operation results in an initial energy cost due to actuation of the tuning mechanism. From figure 12, it can be seen that the amount of energy consumed during the tuning operation is larger for those source frequencies (13, 22 Hz) that are relatively farther from the untuned frequency of the cantilevers in the tunable device (approximately 18 Hz), as the actuator consumes more power to provide the necessary magnetic stiffness necessary to tune to these frequencies. In addition, the net power output is lower than the power output at frequencies closer to the untuned resonance frequency of the device (see figure 11) due to the introduction of more mechanical damping (see figure 8). Hence, more time is necessary to recover the energy spent on tuning for the tunable array to eventually exceed

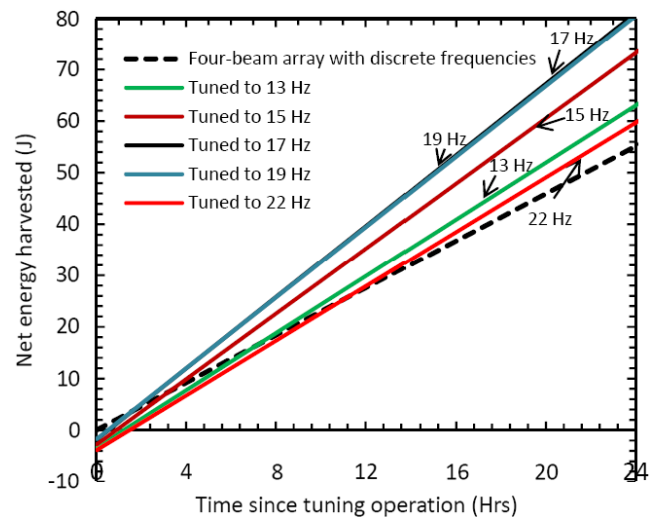


Figure 12. Net energy harvested by the tunable energy harvesting device (tuned to different resonant frequencies within the effective bandwidth of the device), accounting for the energy consumed initially to tune the device.

the net energy harvested by the discrete beam array. For smaller frequency tuning adjustments the energy required for the tuning mechanism is smaller and the effective output of the tunable energy harvesting device is larger, hence, much less time is required for the tunable beam array to outperform the discrete beam array in terms of net energy harvested. (Note that the specific times calculated in this analysis are dependent on both the design of the discrete beam array and the amplitude of the source vibration.)

5. Discussion and conclusions

A self-tunable energy harvesting methodology that utilizes a magnetic force resonance frequency tuning technique is presented for autonomous energy harvesting device

development for powering wireless sensors. The tuning technique is programmed using LabView to allow the device to tune to various source frequencies within its frequency bandwidth. In this work, the root mean square (rms) of peak power output is considered as the cut-off power to determine the frequency tunable range of the device. The device was successfully tuned from -27% to $+22\%$ of the untuned resonance frequency of the beam array, while outputting a power of approximately 0.7–1 mW. The 49% bandwidth obtained for this prototype device using the magnetic force resonance frequency tuning technique provides a basis for future energy harvesting device development for broad frequency range applications. An additional advantage of the magnetic stiffness tuning approach is that the technique is semi-active and does not require any electrical energy to maintain at its tuned resonance frequency.

There have been several approaches that were presented in the literature for developing autonomous energy harvesting devices for powering wireless sensors; for example Ferrari *et al* [30] have presented a battery-less sensor module that has a piezoelectric energy harvesting device for passive sensors consuming approximately 205 W of peak power while transmitting data. Torah *et al* [31] have demonstrated a self-powered autonomous node which adjusts the measurement/transmit duty cycle according to the available energy. In addition, Elfrink *et al* have developed an autonomous wireless sensor node that is powered by a vacuum-packaged piezoelectric MEMS energy harvester [32].

In these earlier works the authors were seeking ways to reduce the energy consumption and requirements for the system, which could involve reductions in the energy necessary to collect, manipulate, or transmit the data collected from a distributed sensor network. However, in these autonomous devices it was considered that the energy harvesting device was in resonance, which is an assumption which may not always be true in most realistic applications. In the current work we have discussed the self-tuning methodology to address the challenge of matching the energy harvesting device frequency to the source frequency, which is necessary to ensure that the energy harvesting system is generating optimal energy output for a given source vibration environment. Taken together, the reduction of the local energy requirements of the sensor network node combined with an increase in electrical energy generated for a given vibration environment will maximize the performance and effectiveness of the autonomous sensing device.

As these devices would be employed in remote locations that would have different source frequencies which may change their frequencies over time, it is important to consider and address the major challenge of frequency tunability in energy harvesting as part of autonomous device development. Recently, Lallart *et al* [33] have presented a self-tuning scheme for broadband energy harvesting which is of great importance for autonomous system development. While the device in that work is self-tunable, the tunable range of the device is limited as the tuning technique employed is an active tuning technique, which would consume a continuous power output to have the device at a tuned frequency. It is to be noted that even

though the active techniques can successfully tune the energy harvesting device to a wide frequency bandwidth, the amount of energy required to induce the stiffness would increase proportionally, hence the net energy output is compromised. In this work, we have employed a semi-active magnetic force tuning technique that both increases the frequency bandwidth and consumes energy only for initial tuning purposes and which would remain inactive over time enabling higher net power output. The presented methodology is also compared to a discrete beam array to show that over a period of time, the net energy produced by such a technique is higher. The presented methodology would be beneficial to employ for sources that have change in their frequency intermittently over time. It is to be noted that the self-tuning technique would be of limited effectiveness if the source frequency changed continuously, as the energy consumed by each tuning step would decrease the net power output harvested by the device.

The approach described here is a first step in the direction of having an autonomous energy harvesting device with semi-active self-tuning capability that can tune to source frequencies within a given permissible range. In this initial prototype we note that an external power source (provided by the USB port of the DAQ card) is used to power the actuator, and a computer running Labview (rather than a standalone microprocessor) is used to perform the magnetic tuning operation. In addition, the optimal load resistances for maximum power output (as shown in figure 7(b)) were altered manually. For a truly autonomous, standalone device ultimately all power necessary for the entire system, including frequency tuning, communication, and logic, would need to be supplied by the energy harvested by the device (this work is currently under development and will be published elsewhere).

In terms of system-level design, the amount of energy harvested versus the number of times the frequency tuning is performed has to be logistically determined and an application specific algorithm has to be built to allow effective device tuning and power output. In particular, given the recent achievements in ultralow-power electronic circuitry specifically developed for energy harvesting applications, it is ultimately envisioned that a practical system would entail the following. First, the device would be in a deep-sleep mode where power is continuously harvested at a given device state (frequency), with periodic wakeup times where the autonomous system checks the source frequency. The autonomous system then determines whether a new tuning step is warranted to enhance the device performance (if, for example, the source frequency has changed since the last tuning operation). If so desired, the device performs the tuning step, after which the system goes back into deep-sleep (ultralow-power) mode and continuously harvests energy until the next programmed periodic check. In such applications a system-level 'energy check-book' must continuously be monitored that weighs energy expenditures (such as tuning operations) versus improvement in harvesting device performance to ensure that ultimately a net energy gain is available for the ultimate intended use. In this manner the development of efficient and reliable mechanisms providing autonomous self-tuning capabilities to energy harvesting

devices will broaden the environments and energy harvesting approaches that can be utilized for various applications.

Acknowledgment

The authors acknowledge the help with experimentation provided by undergraduate student Kevin Heaney, supported by the Stevens Summer Scholars Program.

References

- [1] Roundy S, Wright P K and Pister K S J 2002 Micro-electrostatic vibration-to-electricity converters *Proc. ASME Int. Mechanical Engineering Congr. Exposition* pp 487–96
- [2] Mitcheson P D, Miao P, Stark B H, Yeatman E M, Holmes A S and Green T C 2004 MEMS electrostatic micropower generator for low frequency operation *Sensors Actuators A* **115** 523–9
- [3] Chiu Y, Kuo C T and Chu Y S 2007 MEMS design and fabrication of an electrostatic vibration-to-electricity energy converter *Microsyst. Technol.* **13** 1663–9
- [4] Williams C B, Shearwood C, Harradine M A, Mellor P H, Birch T S and Yates R B 2001 Development of an electromagnetic micro-generator *IEE Proc.: Circuits, Devices Syst.* **148** 337–42
- [5] Glynne-Jones P, Tudor M J, Beeby S P and White N M 2004 An electromagnetic, vibration-powered generator for intelligent sensor systems *Sensors Actuators A* **110** 344–9
- [6] Beeby S P, Torah R N, Tudor M J, Glynne-Jones P, O'Donnell T, Saha C R and Roy S 2007 A micro electromagnetic generator for vibration energy harvesting *J. Micromech. Microeng.* **17** 1257–65
- [7] Roundy S and Wright P K 2004 A piezoelectric vibration based generator for wireless electronics *Smart Mater. Struct.* **13** 1131–42
- [8] Ericka M, Vasic D, Costa F, Poulin G and Tliba S 2005 Energy harvesting from vibration using a piezoelectric membrane *J. Physique IV* **128** 187–93
- [9] Kim S, Clark W W and Wang Q M 2005 Piezoelectric energy harvesting with a clamped circular plate: analysis *J. Intell. Mater. Syst. Struct.* **16** 847–54
- [10] Kim S, Clark W W and Wang Q M 2005 Piezoelectric energy harvesting with a clamped circular plate: experimental study *J. Intell. Mater. Syst. Struct.* **16** 855–63
- [11] Fang H B, Liu J Q, Xu Z Y, Dong L, Wang L, Chen D, Cai B C and Liu Y 2006 Fabrication and performance of MEMS-based piezoelectric power generator for vibration energy harvesting *Microelectron. J.* **37** 1280–4
- [12] Kuehne I, Marinkovic D, Eckstein G and Seidel H 2008 A new approach for MEMS power generation based on a piezoelectric diaphragm *Sensors Actuators A* **142** 292–7
- [13] Liu J Q, Fang H B, Xu Z Y, Mao X H, Shen X C, Chen D, Liao H and Cai B C 2008 A MEMS-based piezoelectric power generator array for vibration energy harvesting *Microelectron. J.* **39** 802–6
- [14] Renaud M, Karakaya K, Sterken T, Fiorini P, Van Hoof C and Puers R 2008 Fabrication, modelling and characterization of MEMS piezoelectric vibration harvesters *Sensors Actuators A* **145/146** 380–6
- [15] Shen D, Park J H, Ajitsaria J, Choe S Y, Wickle H C and Kim D J 2008 The design, fabrication and evaluation of a MEMS PZT cantilever with an integrated Si proof mass for vibration energy harvesting *J. Micromech. Microeng.* **18** 055017
- [16] Wang L and Yuan F G 2008 Vibration energy harvesting by magnetostrictive material *Smart Mater. Struct.* **17** 045009
- [17] Berbyuk V and Sodhani J 2008 Towards modelling and design of magnetostrictive electric generators *Comput. Struct.* **86** 307–13
- [18] Challa V R, Prasad M G and Fisher F T 2009 A coupled piezoelectric–electromagnetic energy harvesting technique for achieving increased power output through damping matching *Smart Mater. Struct.* **18** 095029
- [19] Stanton S C, McGehee C C and Mann B P 2010 Nonlinear dynamics for broadband energy harvesting: investigation of a bistable piezoelectric inertial generator *Physica D* **239** 640–53
- [20] Lin J T, Lee B and Alphenaar B 2010 The magnetic coupling of a piezoelectric cantilever for enhanced energy harvesting efficiency *Smart Mater. Struct.* **19** 045012
- [21] Gieras J F, Oh J H, Huzmezan M and Sane H S 2007 Electromechanical energy harvesting system *Patent Publication Numbers* WO2007070022(A2), WO2007070022(A3)
- [22] Wu X, Lin J, Kato S, Zhang K, Ren T and Liu L 2008 A frequency adjustable vibration energy harvester *Power MEMS 2008 + microEMS2008 (Sendai)* pp 245–8
- [23] Roundy S and Zhang Y 2005 Toward self-tuning adaptive vibration based micro-generators *Proc. SPIE—Int. Soc. Opt. Eng.* **5649** 373–84
- [24] Remtema T and Lin L 2001 Active frequency tuning for micro resonators by localized thermal stressing effects *Sensors Actuators A* **90** 326–32
- [25] Leland E S and Wright P K 2006 Resonance tuning of piezoelectric vibration energy scavenging generators using compressive axial preload *Smart Mater. Struct.* **15** 1413–20
- [26] Challa V R, Prasad M G, Shi Y and Fisher F T 2008 A vibration energy harvesting device with bidirectional resonance frequency tunability *Smart Mater. Struct.* **17** 015035
- [27] Marzencki M, Defosseux M and Basrour S 2009 MEMS vibration energy harvesting devices with passive resonance frequency adaptation capability *J. Intell. Mater. Syst. Struct.* **18** 1444–53
- [28] Zhu D, Tudor M J and Beeby S P 2010 Strategies for increasing the operating frequency range of vibration energy harvesters: a review *Meas. Sci. Technol.* **21** 022001
- [29] Nakano K, Elliott S J and Rustighi E 2007 A unified approach to optimal conditions of power harvesting using electromagnetic and piezoelectric transducers *Smart Mater. Struct.* **16** 948–58
- [30] Ferrari M, Ferrari V, Guizzetti M and Marioli D 2009 An autonomous battery-less sensor module powered by piezoelectric energy harvesting with RF transmission of multiple measurement signals *Smart Mater. Struct.* **18** 085023
- [31] Torah R, Glynne-Jones P, Tudor M, O'Donnell T, Roy S and Beeby S 2008 Self-powered autonomous wireless sensor node using vibration energy harvesting *Meas. Sci. Technol.* **19** 125202
- [32] Elfrink R et al 2009 First autonomous wireless sensor node powered by a vacuum-packaged piezoelectric MEMS energy harvester *IEDM: Technical Digest—Int. Electron Devices Mtg* 5424300 22.5.1–4
- [33] Lallart M, Anton S R and Inman D J 2010 Frequency self-tuning scheme for broadband vibration energy harvesting *J. Intell. Mater. Syst. Struct.* **21** 897–906